Geomech. Geophys. Geo-energ. Geo-resour. (2023) 9:158
https://doi.org/10.1007/s40948-023-00702-4

ORIGINAL ARTICLE

Mechanical and electrical responses of natural-cooled high-temperature granite of different grain sizes

Peng Jia · Yijin Qian · Qiwei Wang · Songze Mao · Jialiang Lu

Received: 26 July 2022 / Accepted: 26 November 2023

Abstract In order to understand the effect of grain size on the mechanical and electrical responses of natural-cooled high-temperature granite, uniaxial compression tests were carried out on natural cooled coarse- and fine-grained granite samples subjected to thermal treatment at room temperature, 200 °C, 400 °C, and 600 °C respectively. The resistivity and acoustic emission (AE) during the compression were monitored and changes in physical and mechanical properties, the AE and resistivity characteristics in the loading process were analyzed. Results show that high temperature exerts a more significant effect on deteriorating the coarse-grained granite. Changes in resistivity can reflect the development of rock damage. Corresponding to the compaction stage, crack initiation and stable propagation stage, and crack rapid propagation stage of rock under compressive load, changes in resistivity can be divided into three stages accordingly, including the initial rapid descent stage, the gentle descent stage, and the secondary rapid descent stage for the thermal-treated rock at 25–400 °C. The secondary rapid descent stage of resistivity can be used as a precursor for rock entering into the failure stage. The resistivity change is more sensitive to the damage development in coarse-grained granite.

Highlights

- Influences of grain sizes on the changing rule of electrical resistivity during the fracturing processes of thermal-damaged granite samples were obtained.
- The resistivity precursors of coarse- and fine-grained granite under compression were obtained.
- The damage mechanism of granite can be reflected through the electrical resistivity change in the failure stage.

Keywords High temperature · Granite · Damage · Electrical resistivity

1 Introduction

Hot dry rocks (HDRs) are the host strata for geothermal resource exploitation, and granite is the most widely distributed type of HDRs (Zhu et al. 2021, 2020; Li et al. 2021; Zhao et al. 2021; Zhang et al. 2020; Kim et al. 2014; Ersoy et al. 2021). Therefore, studying physical and mechanical properties of high-temperature granite is significant for the extraction of thermal energy from HDRs. The mechanical

P. Jia (✉) · Y. Qian · Q. Wang · S. Mao · J. Lu
School of Resources and Civil Engineering, Northeastern University, NO. 3-11, Wenhua Road, Heping District, Shenyang 110819, China
e-mail: polorjia@163.com

Published online: 02 December 2023

properties of granite are dependent on fractures inside the rock (Griffiths et al. 2017). Generally, physical changes inside granite under thermal treatment can be divided into four stages: the evaporation of water, the compaction of fractures under thermal expansion of grains, development of intergranular fractures due to high temperatures, and development of transgranular fractures due to high temperatures (Li et al. 2020; Gautam et al. 2021; Yang et al. 2017). Gautam explored the physical parameters, microstructures, and mineral characterization of granite subjected to cyclic heating and cooling, and the results indicate that the increasing number of thermal cycles induces strain accumulation inside granite (Gautam et al. 2021). Combining acoustic emission (AE) monitoring and digital image correlation, Miao discussed crack development modes of Beishan granite subjected to thermal treatment at different temperatures under uniaxial compression, and results indicate that tensile cracks mainly appear at a relatively low temperature in the granite, while shear cracks gradually become dominant as the temperature rises (Miao et al. 2021). Ma conducted real-time triaxial compression tests on high-temperature granite to study influences of the thermal effect and transverse stress on mechanical properties of the rock (Ma et al. 2020). Results suggest that the brittleness of granite changes with the rising temperature and transverse stress. Wang studied influences of different heating rates on mechanical properties of Eibenstock granite (Wang et al. 2019). Results show that the heating rate insignificantly influences the tangent elastic modulus and uniaxial compressive strength of granite, while the highest temperature significantly affects the two.

It is known that the grain size of granite plays an important role in the homogeneity of the rock, and the contact surface between grains has certain strength (Yin et al. 2021). However, different thermal expansion of grains at high temperatures may induce uncoordinated deformation among grains, thus causing damage. For example, the thermal expansion of feldspar is four times as much as that of quartz at the same temperature (Tripathi et al. 2021). Through X-ray fluorescence spectrometry analysis, Kang obtained the variation coefficient of granite and found that the coefficient increases if the grains are distributed unevenly, which causes the early development of thermal damage leading to the deterioration of strength (Kang et al. 2021). Shao tested the deformation of Strathbogie granite with three different grain sizes after thermal shock (Shao et al. 2014). The research revealed that under the same thermal shock conditions, the grain size does not exert remarkable influences on the elastic modulus at temperatures below 400 °C while the finer the grains are, the larger the elastic modulus at temperatures higher than 400 °C.

The crack initiation and propagation in rocks may induce AE events in the loading process, and are used to understand the fracture process of rocks and attain precursors for fracture (Lockner 1993; Ishida et al. 2017; Hall et al. 2006). Kumari performed AE monitoring of the tension process of high-temperature granite and pointed out that numerous fractures are closed inside rocks as the temperature rises thus making the rocks become instable (Kumari et al. 2019). Zhao investigated AE properties of thermal-treated granite in shear process and found that microcracks in the rock open and close multiple times, however, the number of total opening events of microcracks is higher than that of the closure events after reaching a certain stress level (Zhao et al. 2019). Tian simulated the uniaxial loading process of granite of different grain sizes after thermal treatment by using the Particle Flow Code 2D (PFC2D) and concluded that the larger the grain size, the more the contact surface between grains, which is conducive to the crack development (Tian et al. 2018, 2020).

Due to the existence of many multi-scale defects from microscopic to mesoscopic and even to macroscopic scales in rocks, changes in porosity and pore structures, and the development, propagation, and coalescence of defects such as pores and fractures in rocks in the loading process will inevitably cause the variation of the structural characteristics of rocks, leading to the variations in the resistivity of rocks. Therefore, a number of scholars studied damage and fracture processes of rocks by measuring the resistivity of rocks during the loading process (Roy 2020; Parkhomenko 2012). As early as in the 1960s, Brace et al. applied geoelectrical surveying to monitor rock fracturing process and found that resistivity can effectively reflect the development of cracks in rocks under loading (Brace et al. 1965; Brace and Orange 1968a, 1968b; Brace 1975). Then, Parkhomeko et al. discovered that fracture closure in rocks in the loading process can be well characterized by changes in resistivity (Parkhomenko 2012, 1982). Jia et al. (2020)

found there exists close correlation between resistivity change and the crack development, and provided a method for identifying potential fracture planes based on the anisotropy of resistivity. Sun studied the relationship between resistivity and rock fracture under uniaxial compression and found that the critical point of rapid resistivity change is at a stress level equal to 75–85% of the peak strength (Sun et al. 2015). Niccolini compared the changes in electrical resistance during the fracture of different types of rock, and found that all three types of rock show a significant sudden change in electrical resistance prior to fracture (Niccolini et al. 2020). Guo measured the resistivity of cemented gangue backfill under uniaxial compression and found that the resistivity curve resembles a U-shaped change and deemed that the flat section can be used as the precursor for failure of the backfill material (Guo et al. 2021). Li compared AE activities and resistivity changes of sandstone under uniaxial compression and found that the resistivity is more sensitive to structural changes of rock in the compaction and elastic stages (Li et al. 2014).

Although scholars have conducted a large number of studies on the physical and mechanical properties of high-temperature rocks and have achieved fruitful results, there have been few studies on the influence of granite particle size on the mechanical and electrical properties of thermal-damaged rocks, which is of great significance in monitoring rock failure using electrical methods. Considering this, we carried out real-time monitoring on resistivity and AE events of thermal-damaged granite of two different grain sizes under uniaxial compression. Effect of temperature and grain sizes on physical and mechanical properties as well as the changing rule of resistivity were analyzed. The superiority of resistivity monitoring in prediction of damage and fracture mechanisms of the rock was also discussed.

2 Sample preparation and test methods

2.1 Sample preparation

Fine-grained granite collected from a mine in Jinzhou City (Liaoning Province, China) and coarse-grained granite taken from a mine in Changsha City (Hunan Province, China) were machined into

Fig. 1 Fine- and coarse-grained granite samples

samples measuring φ50 mm × 100 mm (Fig. 1) following recommendations of the International Society for Rock Mechanics (ISRM) (Ishida et al. 2017). Here, the term fine- and coarse-grained granite are only used to distinguish the particle sizes of the two. The upper and lower surfaces of the samples were polished to have parallelism below 0.02 mm. After binarization processing of images of the two types of granite using MATLAB, statistical analysis was conducted on the grain diameter to obtain average grain diameters of the two types of rocks. The average grain diameters of the coarse- and fine-grained granite were 5.05 and 1.5 mm, respectively, as shown in Fig. 1. To eliminate influences of water in the rock on the physical and mechanical parameters of the rock samples, the prepared and polished rock samples were dried at 105 °C for 48 h.

Then, the density and initial porosity were calculated and the P-wave velocity and initial resistance were tested using HS-Y403B Rock Acoustic Wave Parameter Tester Produced by Xiangtan Tianhong Research Institute in China and the KEITHLY 2470 micro-current real-time monitoring instrument produced by Tektronix in the United States. The peak compressive strength and the elastic modulus were obtained through uniaxial compression test as described in Sect. 2.2. The initial porosity can be obtained by the mass difference of saturated and dry rock sample divided by the sample volume and the density of water. The basic physical and mechanical parameters of the two types of granite samples are listed in Table 1.

Table 1 Mean physical and mechanical parameters of the tested samples

Physical and mechanical parameters	Fine-grained granite	Coarse-grained granite
Density (g/cm^3)	2.59	2.63
P-wave velocity (m/s)	4306 ± 200	3912 ± 100
Initial resistance ($10^7\Omega$)	2.51	4.46
Peak compressive strength (MPa)	145.46	103.01
Elastic modulus (GPa)	26.6	20.6
Initial porosity (%)	0.46	0.76
Average grain diameter (mm)	1.50	5.05

2.2 Thermal treatment and uniaxial loading

The MYC-5 high-temperature chamber-type electric furnace was used to heat the rock samples to 200 °C, 400 °C, and 600 °C separately. Because influences of the heating rate within 10 °C/min on the rock can be ignored (Wang et al. 2019; Kang et al. 2021), the heating rate was set to be 5 °C/min. To ensure sufficient heating of the interior of rock samples, after rising to the preset temperature, the samples were preserved at the temperature for 4 h. To avoid further thermal shock on the rock samples, the heated rock samples were remain in the furnace until to the room temperature. Three parallel tests were conducted for each of the two types of granite at each temperature to ensure the reliability of the test data.

Uniaxial loading tests were carried out on a YAG-3000kN micro-computer-controlled servo press, which is able to provide the maximum vertical test pressure of 3000kN and has the overall stiffness larger than 3 GN/m. The displacement-controlled mode was adopted in the loading at a loading rate of 0.002 mm/s according to the ISRM (Ishida et al. 2017). AE and resistivity of the rock were monitored real-timely during the loading process (Fig. 2). A KEITHLY 2470 Digital Source Meter produced by Tektronix in the United States was used to implement monitoring of changes in electrical resistivity. The Source Meter's maximum measurement voltage is 1100 V and the minimum measurement current is 10 fA. The voltage, current, and sampling frequency were set as 100 V, 100 μA, and 15 times/s separately. A PCI-II AE monitoring system produced by the Petroleum Analyzer Company in the United States was used to monitor the acoustic information in the loading process.The AE threshold was set to be 40 dB.

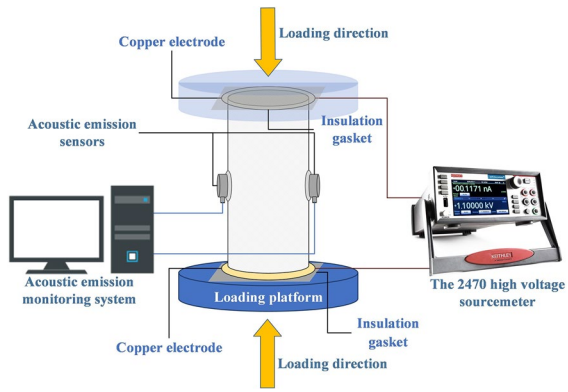

Fig. 2 The uniaxial loading and the resistivity and AE monitoring devices

3 Test results analysis

3.1 Influences of high temperatures on physical parameters of granite

Surface morphologies of the two types of granite treated at different temperatures are illustrated in Fig. 3.As the temperature increases, due to the iron-oxidization and the lost of the crystal water in rock, the color of the granite samples becomes lighter and some light brownish yellow spots appear in local areas (Jia et al. 2021).

By measuring the density before (ρ_0) and after heating (ρ), the density reduction ratio can be obtained through $\frac{\rho-\rho_0}{\rho_0} \times 100\%$ (Fig. 4). The mass loss rates of the two types of granite are approximated when the temperature of thermal treatment is lower than 200 °C, which are 0.0238% and 0.0226% for fine- and coarse-grained granite, respectively. Because when thermal treatment is lower than 200 °C, the mass loss is mainly due to the evaporation

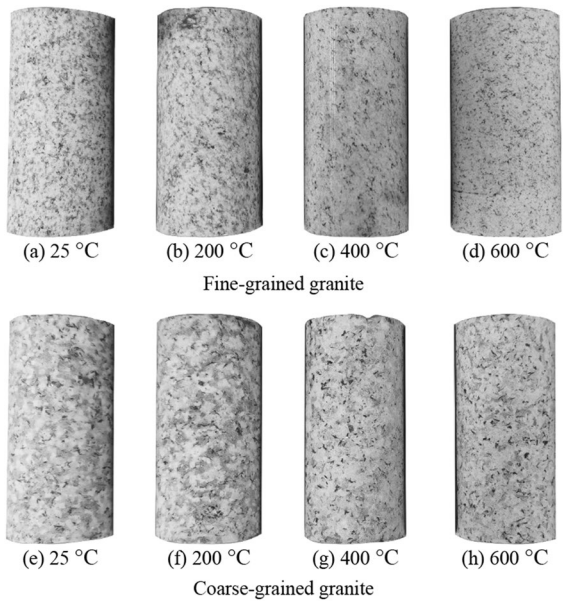

Fig. 3 Natural-cooled high temperature treated granite samples

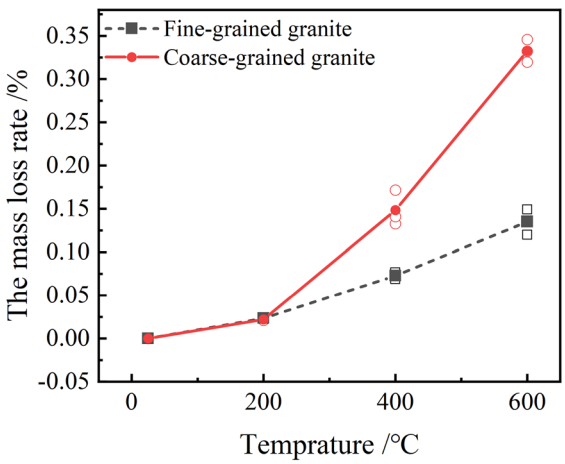

Fig. 4 Relationship between mass loss and temperature

of free water (Wong et al. 2020). When the temperature is over 200 °C, the mass loss rate shows an obvious increase due to the evaporation of free and bound water. Note that the mass loss rate of coarse-grained granite increases rapidly with temperature. At 400 °C and 600 °C, the mass loss rates of coarse-grained granite are 2.31 and 2.26 times than those of fine-grained granite.

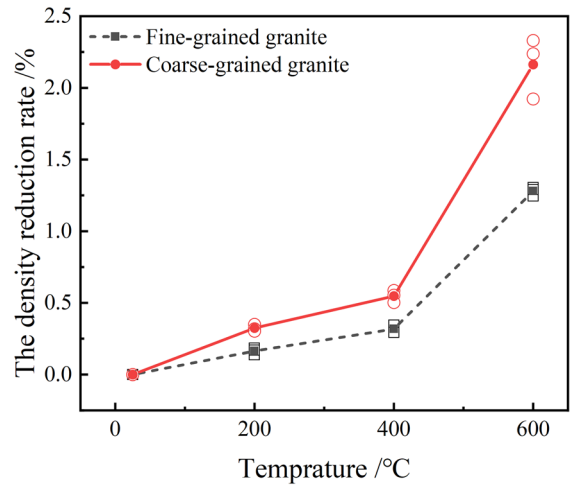

Fig. 5 Relationship between density reduction rate and temperature

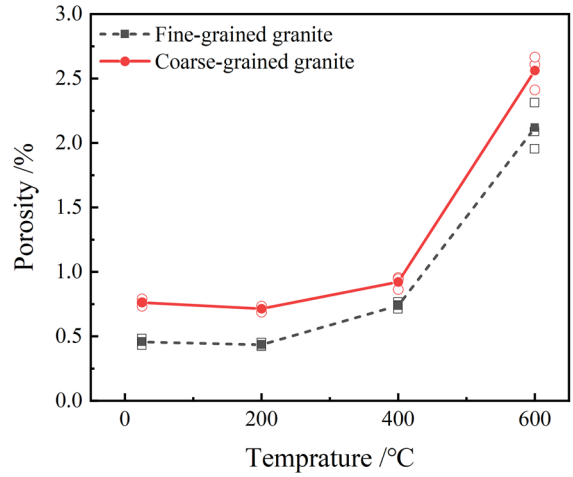

Fig. 6 Relationship between porosity and temperature

Figure 5 shows the density reduction rate with temperature. When the heating temperature is lower than 400 °C, the density of the two types of granite decreases slowly; when over 400 °C, the density reduction rate increase significantly, and the density reduction rate of coarse-grained granite is 2.56 times than that of the fine-grained one. The porosity change of the two types of granite before and after thermal treatment can be calculated through $\frac{m_w - m_{w0}}{\rho_{\text{water}} V} \times 100\%$ as shown in Fig. 6. Where m_{w0} is the mass of the saturated rock sample before thermal treatment, m_w is the

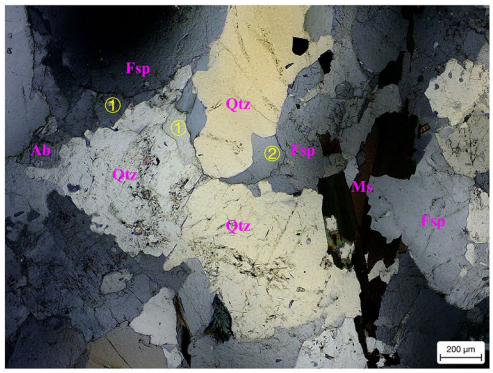

(a) 25 °C coarse-grained granite

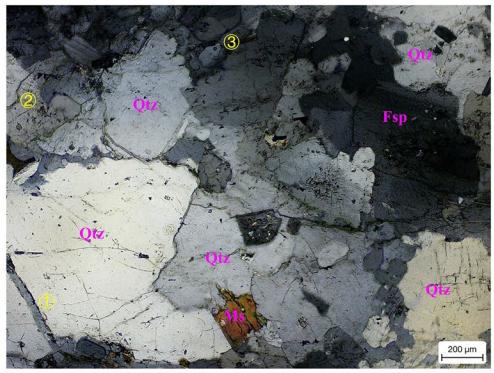

(b) 25 °C fine-grained granite

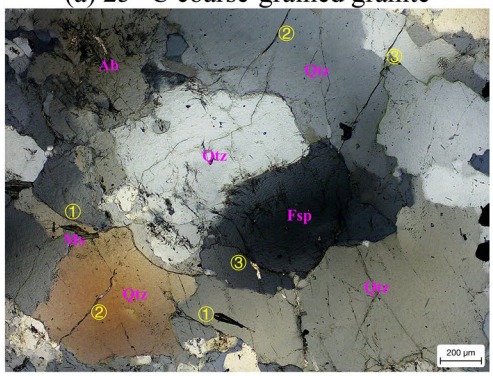

(c) 200 °C coarse-grained granite

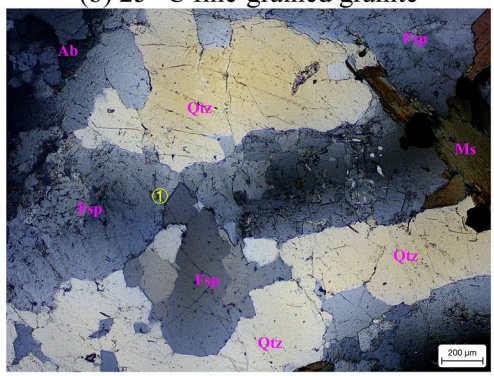

(d) 200 °C fine-grained granite

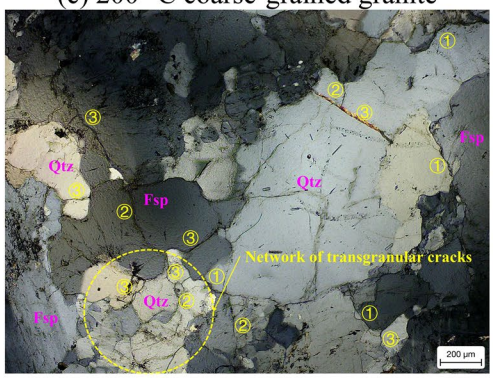

(e) 400 °C coarse-grained granite

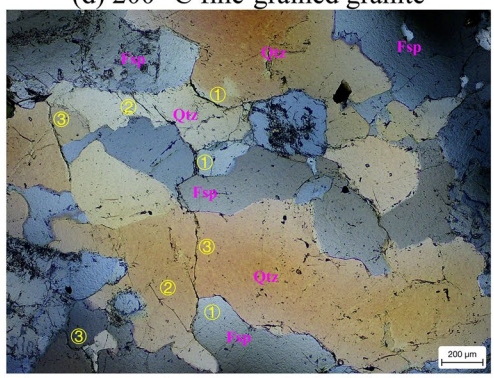

(f) 400 °C fine-grained granite

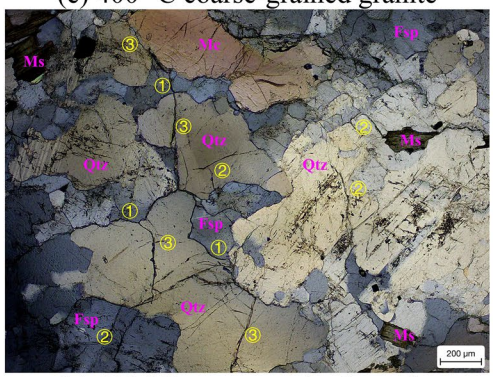

(g) 600 °C coarse-grained granite

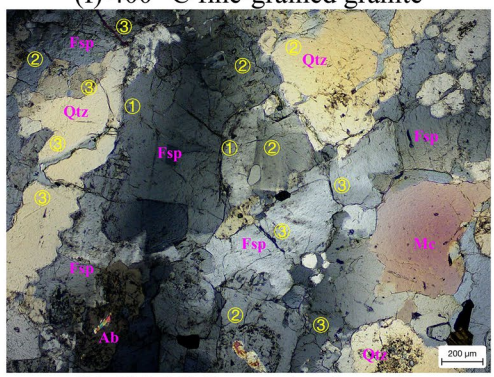

(h) 600 °C fine-grained granite

◂**Fig. 7** The orthogonal polarization micrograph of the fine- and coarse-grained granite. Observed under the orthogonal polarization microscope (ZEISS primotech T/R POL conos)

mass of the saturated rock after thermal treatment, V is the volume of the thermal damaged rock and ρ_{water} is the density of water. It can be seen that when the heating temperature is over 400 °C, porosity in the two types of granite increase rapidly. The main cause for the significant deterioration of physical properties of granite is due to the phase transition of quartz at 573 °C (Yang et al. 2020a; Wang and Konietzky 2019; Zhao et al. 2018) and the uncoordinated thermal expansion among grains, which is more severe in coarse-grained granite.

The orthogonal polarization microscopy images of the two types of granite are illustrated in Fig. 7, in which ①,②, and ③ represent intergranular cracks, intragranular cracks, and transgranular cracks respectively. At 25 °C, coarse- and fine-grained granite samples differ slightly in their microstructures, both have certain initial gaps between mineral grains but intact grains. At 25–200 °C, fine-grained granite becomes more compact due to the thermal expansion and deformation of mineral grains, and the grains are still relatively intact. In this temperature range, cracks between mineral grains are compacted, which corresponding to the slight decrease in porosity at 200 °C as shown in Fig. 6. In comparison, intergranular cracks begin to develop between mineral grains in coarse-grained granite at the temperature, the compactness of mineral grains is lower than that of fine-grained granite, and a few intragranular cracks appear in these grains. In the range of 200–400 °C, intergranular cracks further develop in the two types of granite and mineral grains have more clear boundaries. In addition, intragranular cracks in coarse-grained granite further develop and coalesce to form transgranular cracks. As a result, the integrity of mineral grains is further impaired and some mineral grains are broken into smaller grains under damage of the crack network formed by multiple transgranular cracks. Transgranular cracks also develop in fine-grained granite, while their number is obviously lower than that in coarse-grained granite and mineral grains therein remain intact on the whole. At 400 ~ 600 °C, lots of cracks develop in the two types of granite because of the α-β phase transition of quartz grains (Yang et al. 2020a, 2020b; Wang and Konietzky 2019; Zhao et al. 2018), so mineral grains are broken more seriously. Particularly, there are numerous transgranular cracks in quartz grains. Besides, the width of cracks in coarse-grained granite is larger than that of fine-grained granite, so coarse-grained granite is more severely damaged. The above microscopic analysis reveals that internal damage of the high temperatures in coarse-grained granite is more serious than in fine-grained granite.

3.2 Influences of temperature and grain size on mechanical properties of granite

Stress–strain curves of the two types of granite at different temperatures are shown in Fig. 8. The elastic moduli gradually reduce and the peak strains increase with the rising in temperature. At 400 °C, and 600 °C, the elastic moduli of the two types of granite both decrease significantly, which means that the mechanical properties of granite can be significantly deteriorated over 400 °C. It should be noted that the coarse-grained granite is more significantly deteriorated than fine-grained granite and its stress–strain curve shows a multi-peak phenomenon.

Figure 9 shows influences of temperature on the uniaxial compressive strength of the two types of granite. The peak strength of the fine-grained granite has a first increase and then decrease trend as the temperature rises and reaches the maximum of 180.1 MPa at 200 °C. The most important cause for the increased strength is that thermal expansion of mineral grains enables internal voids to be filled and compacted (Rossi et al. 2018). Afterwards, the strength gradually reduces to 119.29 MPa at 600 °C, showing a decrease by 17.98%. Unlike the fine-grained granite, the peak strength of the coarse-grained granite displays a gradual decline trend. This is because the relatively high initial pores and voids in the coarse-grained granite cannot be sufficiently filled and compacted by the thermal expansion of mineral grains. At 600 °C, the peak strength of coarse-grained granite decreases by 47.17% from 103.01 to 54.42 MPa.

Figure 10 depicts influences of the temperature on the elastic moduli of the two types of granite. The elastic moduli of the two types of granite both decline with the rising temperature. As the temperature rises from 25 to 600 °C, the average elastic modulus of the coarse-grained granite decreases by 60.03% from 23.39 to 9.35 GPa; in comparison, the

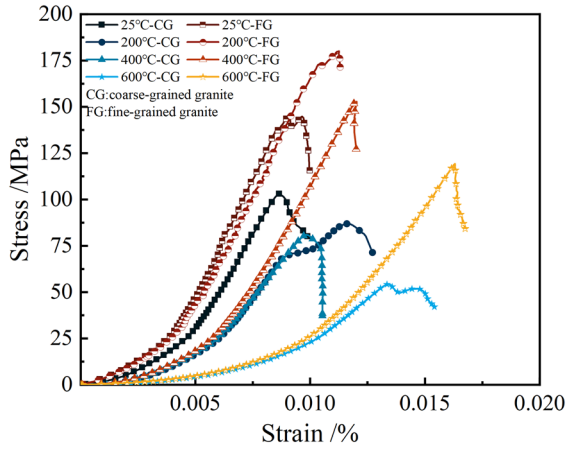

Fig. 8 Stress–strain curves of the fine- and coarse-grained thermal-damaged granite

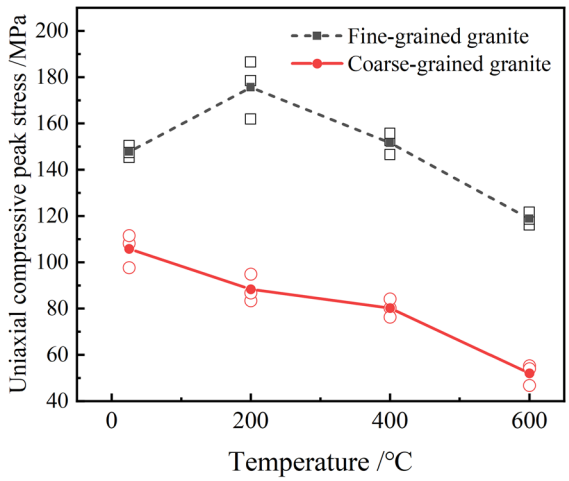

Fig. 9 Relationship between peak strength and temperature of fine- and coarse-grained granite

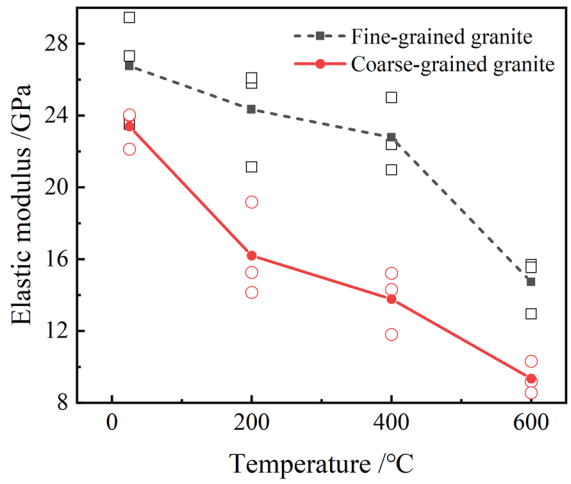

Fig. 10 Relationship between elastic modulus and temperature of fine- and coarse-grained granite

average elastic modulus of the fine-grained granite reduces by 44.97% from 26.75 to14.72 GPa, which is consistent with the research results of Jia et al. (2021) and Xi et al. (2020). High temperature exerts a significant weakening effect on the elastic moduli of the two types of granite, especially for the coarse-grained granite. This can also be manifested by Figs. 5 and 7. Figure 5 shows that the density of the coarse-grained granite decreases more significantly with the increase in the heating temperature. Meanwhile, in Fig. 7, it shows that the thermal-induced cracks in coarse-grained granite are more intense than those of the fine-grained granite. Therefore, the average elastic modulus of coarse-grained granite decreases more substantially than that of the fine-grained granite.

The failure modes of the two types of thermal-damaged granite under uniaxial compression are shown in Fig. 11. For fine-grained granite, the dominate failure mode is the split failure accompanied with plenty of coalesced cracks. For coarse-grained one, shear failure dominants, characterized by a major coalesced crack and fine rock grains on the crack surface. Due to the friction force between the coarse mineral grains on the fracture planes, the interlock effect can be induced (Yang et al. 2020b), so that the post-peak strength of the coarse-grained granite grows and even rebounds. This explains why the stress–strain curve of coarse-grained granite shows the multi-peak phenomenon.

3.3 Influences of high temperature and grain size on resistivity and AE properties

Figure 12 displays the relationships of the cumulative AE counts, average single ringing energy, and resistivity with stress levels. The average single ringing energy $A^{'}$ is defined by Eq. (1) and the resistivity ρ is defined by Eq. (2).

$A^{'}$ represents the average single ringing energy, which indicates the severity of the rupture at the current moment.

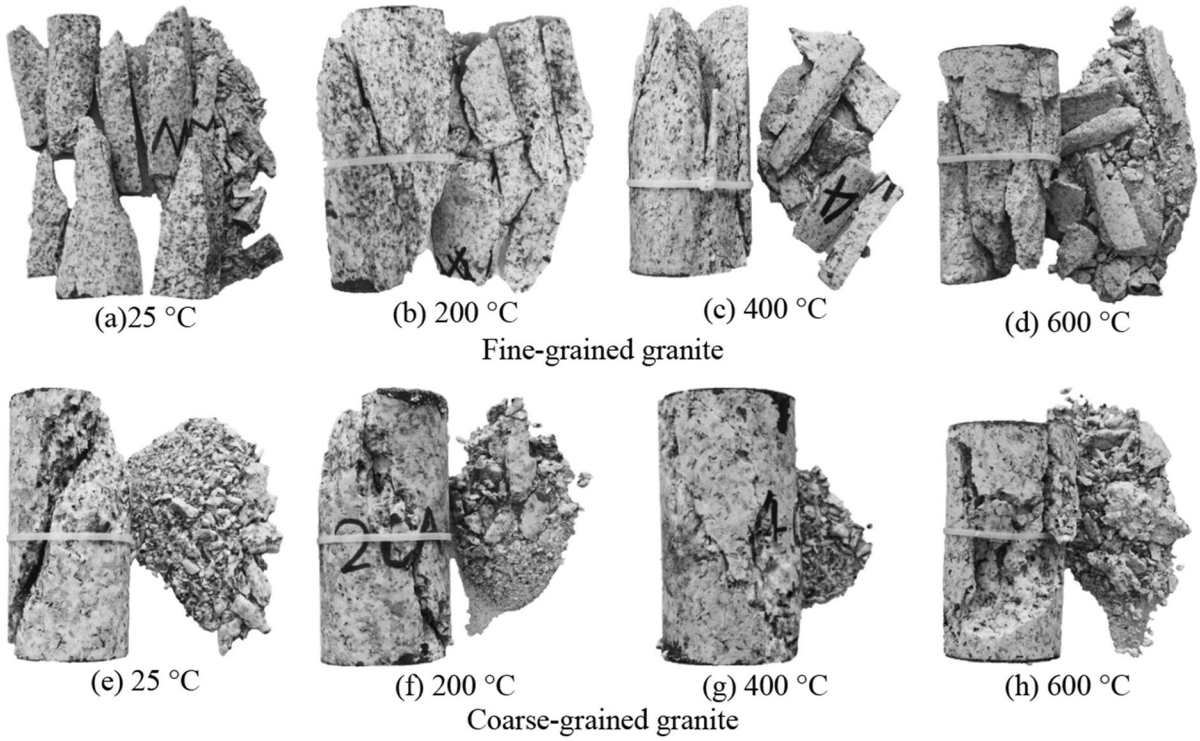

Fig. 11 Failure modes of the thermal-damaged fine- and coarse-grained granite

$$A' = \frac{A}{N} \tag{1}$$

where A and N represent the AE energy and the AE counts at the current moment respectively.

$$\rho = R_t \frac{S_t}{L_t} \tag{2}$$

where R_t and S_t separately denote the resistance and cross-sectional area of the material at time t; L_t represents the length of the material at t.

As shown in Fig. 12, before the peak strength, the resistivity curve can be divided into three stages, that is, the initial rapid descent stage, the gentle descent stage, and the secondary rapid descent stage. Take the accumulative AE counts curve and the resistivity curve in Fig. 12a, b as an example: at 25 °C, the accumulative AE count curve of fine-grained granite ascends rapidly at about 90% of the peak strength; while that of coarse-grained granite increases gently and shows upward trend at about 65% of the peak stress. This indicates that the fine-grained granite displays a significant brittle failure characteristic, while the coarse-grained one exhibits a progressive failure characteristic. While, the resistivity curves of the two types of granite all show an obvious decrease trend in the initial compression stage (lower than 10% of peak stress) due to compaction of the rock, and then all enters into a gentle descent stage. At about 65% of the peak stress, resistivity curves of the two types of granite descend rapidly for the second time, indicating that the rock is undergoing a quick crack propagation stage. So, the secondary fast dorp of resistivity can be seen as a precursor for failure of thermal-damaged granite.

The cause for changes in the internal conductivity of the rock under loading can be illustrated in Fig. 13. The conductivity of dry rock mainly relies on its mineral skeleton; however, the pre-existing voids and fractures (Fig. 13a) cut off some of the conductive paths. When loading, these voids and fractures are compacted and therefore the conductivity of rock is increased (Fig. 13b). This process corresponds to the initial descent stage of resistivity.

With increase of load, the mineral skeletons begin to break, and cracks begin to initiate and propagate,

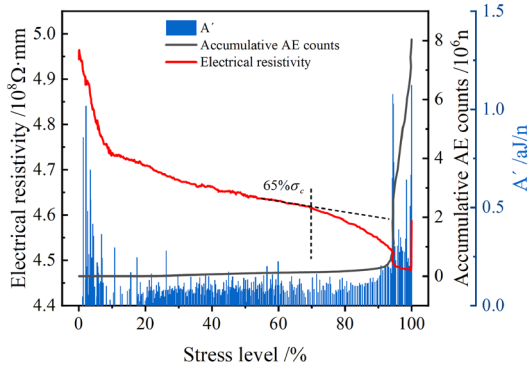

(a) 25 °C fine-grained granite

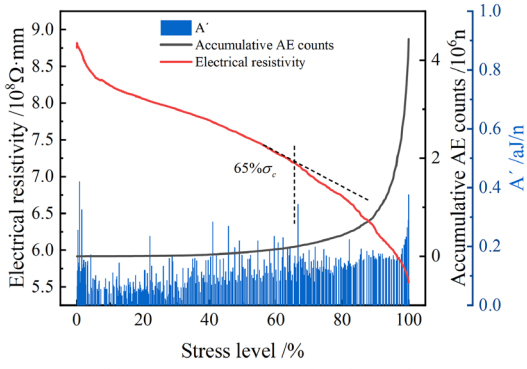

(b) 25 °C coarse-grained granite

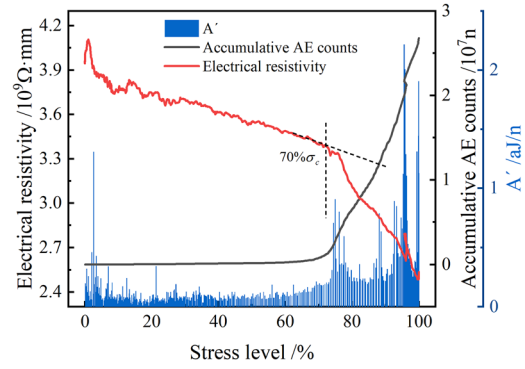

(c) 200 °C fine-grained granite

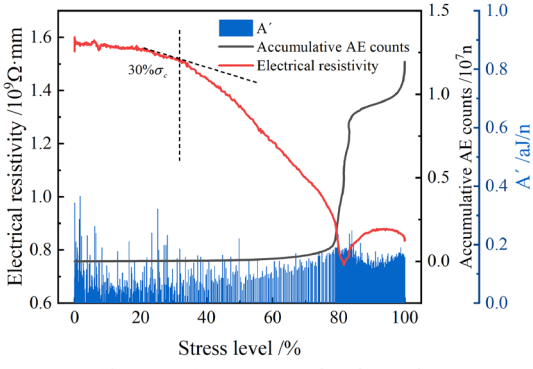

(d) 200 °C coarse-grained granite

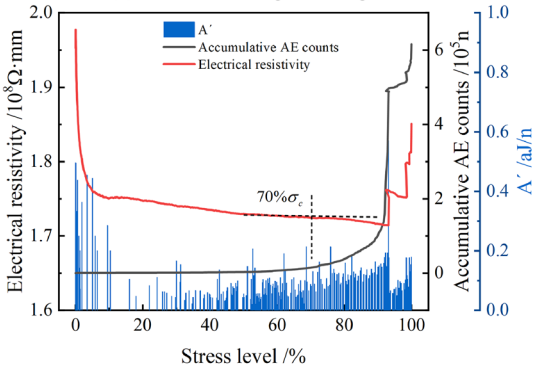

(e) 400 °C fine-grained granite

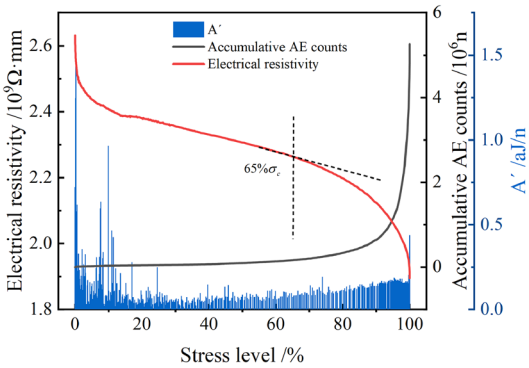

(f) 400 °C coarse-grained granite

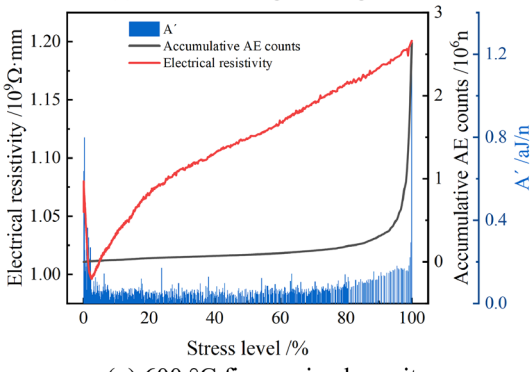

(g) 600 °C fine-grained granite

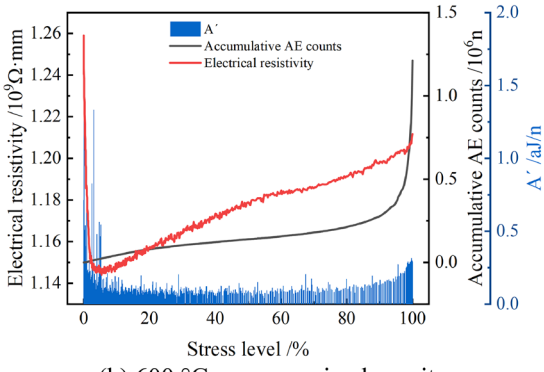

(h) 600 °C coarse-grained granite

◂**Fig. 12** Relationship between resistivity, cumulative AE count, average single ringing energy and stress level

accompanied by the sliding and mutual extrusion of grains (Wang and Konietzky 2019). The conductivity continues to decrease slowly, which corresponds to the gentle descent stage of resistivity (Fig. 13c).

Then cracks enter into the rapid propagation and coalescence stage, and mineral skeleton is rapidly compacted, so the conductivity rises significantly (Fig. 13d). Therefore, the resistivity curve comes to the secondary rapid descent stage. With the occurrence of through cracks, the rock is broken and the conductive paths are cut off completely, resulting in an abrupt increase in resistivity in the final failure stage (Fig. 13e).

Compared with that at 25 °C, when rises to 200 °C, the curve of accumulative AE count of fine-grained granite begins to ascend significantly at about 75% of the peak stress (90% of peak stress at 25 °C) (Fig. 12c); while the significantly ascending stage of accumulative AE count curve of coarse-grained granite (Fig. 12d) still begins at about 80% of the peak stress. This indicates that the thermal treatment leads to a more severe deterioration in the fine-grained granite than in the coarse-grained one, thus causing the decrease of its brittleness. It is worth noting here that the secondary rapid descent stage of resistivity occurs at about 75% and 37% of the peak stress for fine- and coarse-grained granite respectively (both corresponding to the abrupt increase of $A^{'}$), while the surging of the accumulative AE counts does not occur until to 75% and 80% of the peak stress respectively. This indicates that compared with AE, the quick crack development in rock can be early reflected through the onset of the secondary rapid descent of resistivity, and can be used as a precursor for rock entering into the pre-failure stage.

As temperature rises to 400 °C (Fig. 12e, f), the decreasing rate in resistivity of fine- and coarse-grained granite in the compaction stage both shows a significance increase. This is because the aggravated thermal damage in rock promote the quick compaction of mineral skeleton under compression, thus leading to the rapid increase of conductivity. Meanwhile, the secondary descent stage of resistivity curve occurs early than the surge point of the accumulative AE curve both for the fine- and coarse-grained granite. For coarse-grained granite, the secondary descent stage occurs at lower stress level than the fine-grained granite, indicating that the resistivity change is more sensitive in coarse-grained granite.

The secondary descent stage of resistivity and the ascent of the curve of cumulative AE count of fine-grained granite both begin at about 70% of the peak stress; in comparison, the resistivity of coarse-grained granite enters the secondary descent stage at about 65% of the peak stress and its curve of cumulative AE count begins to increase significantly at about 85% of peak stress. It is evident that the resistivity is more sensitive to the damage in coarse-grained granite, which is more heterogeneous than the fine-grained one.

At 600 °C, as shown in Fig. 12g and h, the resistivity of the two types of granite decreases rapidly in the initial compaction stage, followed by a constant increase with loading. It should be note that at 600 °C, there are no failure precursors for the two types of granite. Because the interior of the rock is seriously damaged due to high temperature, and cracks begin to open upon loading, thus leading to the continuously increase in the resistivity. The curves of accumulative AE counts of the two types of granite ascend slowly, indicating the progressive failure characteristics of the two types of granite.

It is worth noting that in the failure stage, the change of resistivity of fine- and coarse-grained granite samples exhibit different trends. Resistivity of fine-grained granite increases abruptly while that of coarse-grained one decreases sharply, which is related to the failure modes of the two types of granite (Fig. 11). Fine-grained granite mainly shows a split failure featured by tensile cracks, and the opening of the macrocracks directly leading to the sharply increase of resistivity; whereas, coarse-grained granite exhibits shear-slip failure and the close contact of the mineral grains on the slip planes causing the rapid reduction in the resistivity. So, the changing trend of resistivity at the failure stage can to some extent reflect the failure mechanism of rock.

4 Conclusions

Uniaxial compression tests were conducted on granite samples with different grain sizes, which were subjected to thermal treatment at the 25 °C, 200 °C, 400 °C, and 600 °C separately before loading. Both

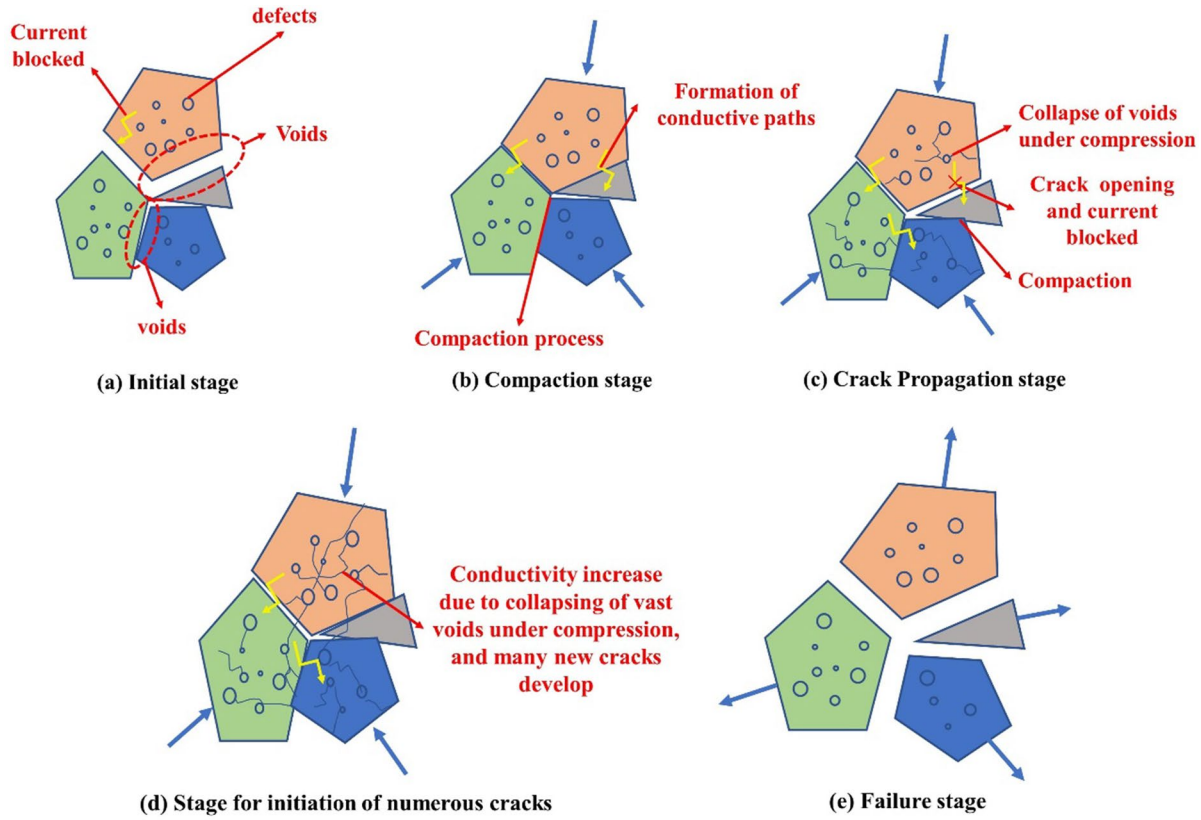

Fig. 13 Schematic diagram for the change of conductivity of rock mineral skeleton

the resistivity and AE information were real-time monitored in the loading process. Influences of temperatures and rock grain sizes on physical and mechanical properties of granite samples were analyzed and the electrical and acoustic emission characteristics of the two types of thermal-damaged granite were discussed. The conclusions are as follows:

1. For fine-grained granite, at 200 °C, the voids can be filled and compacted by the expansion of mineral grains, causing a slightly increase in its peak strength. When temperature is over 400 °C, the mechanical properties of both the fine- and coarse-grained granite are all significantly deteriorated, especially for the coarse-grained granite.
2. Resistivity changes can reflect the development of the internal damage in rock. Corresponding to the compaction stage, crack initiation and stable propagation stage, and crack rapid propagation stage of the rock under compressive load, changes in resistivity can be divided into three stages for the thermal-treated rock at 25–400 °C accordingly, including the initial rapid descent stage, the gentle descent stage, and the secondary rapid descent stage. The secondary rapid descent stage of resistivity can be used as a precursor for rock entering into the failure stage.
3. Changes in resistivity in the failure stage can to some extent reflect the failure mechanism of the rock. If electrodes are placed on the upper and lower faces of the rock samples, tensile failure exhibits a sharp increase in resistivity, while shear failure exhibits an abrupt decrease in resistivity. The resistivity change is more sensitive to the damage development in coarse-grained granite.

Acknowledgements This work was supported by the National Natural Science Foundation of China (52174071), and

the National Key R&D Program of China (2022YFC2903903). The authors are grateful for these supports.

Declarations

Completing interests The authors declare that they have no known competing financial interests or personal relationships that could have appeared to influence the work reported in this paper.

References

Brace WF, Orange AS (1968a) Further studies of the effects of pressure on electrical resistivity of rocks. J Geophys Res 73(16):5407–5420. https://doi.org/10.1029/JB073i016p05407

Brace WF, Orange AS (1968b) Electrical resistivity changes in saturated rocks during fracture and frictional sliding. J Geophys Res 73(4):1433–1445. https://doi.org/10.1029/JB073i004p01433

Brace WF, Orange AS, Madden TR (1965) The effect of pressure on the electrical resistivity of water-saturated crystalline rocks. J Geophys Res 70(22):5669–5678. https://doi.org/10.1029/JZ070i022p05669

Brace WF (1975) Dilatancy-related electrical resistivity changes in rocks. In: Earthquake prediction and rock mechanics, Birkhäuser, Basel, pp 207–217

Ersoy H, Karahan M, Kolaylı H, Sünnetci MO (2021) Influence of mineralogical and micro-structural changes on the physical and strength properties of post-thermal-treatment clayey rocks. Rock Mech Rock Eng 54(2):679–694. https://doi.org/10.1007/s00603-020-02282-1

Gautam PK, Dwivedi R, Kumar A, Kumar A, Verma AK, Singh KH, Singh TN (2021) Damage characteristics of jalore granitic rocks after thermal cycling effect for nuclear waste repository. Rock Mech Rock Eng 54(1):235–254. https://doi.org/10.1007/s00603-020-02260-7

Griffiths L, Heap MJ, Baud P, Schmittbuhl J (2017) Quantification of microcrack characteristics and implications for stiffness and strength of granite. Int J Rock Mech Min Sci 100:138–150. https://doi.org/10.1016/j.ijrmms.2017.10.013

Guo YX, Zhao YH, Feng GR, Ran HY, Zhang YJ (2021) Study on damage size effect of cemented gangue backfill body under uniaxial compression. Chin J Rock Mech Eng 40(12):2434–2444. https://doi.org/10.13722/j.cnki.jrme.2021.0527. (**in Chinese**)

Hall SA, Sanctis FD, Viggiani G (2006) Monitoring fracture propagation in a soft rock (Neapolitan Tuff) using acoustic emissions and digital images. Pure Appl Geophys 163(10):2171–2204. https://doi.org/10.1007/s00024-006-0117-z

Ishida T, Labuz JF, Manthei G, Meredith PG, Nasseri MHB, Shin K, Yokoyama T, Zang A (2017) ISRM suggested method for laboratory acoustic emission monitoring. Rock Mech Rock Eng 50(3):665–674. https://doi.org/10.1007/s00603-016-1165-z

Jia P, Li L, Liu DQ, Wang XS, Wang DC (2020) Insight into rock crack propagation from resistivity and ultrasonic wave variation. Theoret Appl Fract Mech 109:102758. https://doi.org/10.1016/j.tafmec.2020.102758

Jia P, Yang QY, Liu DQ, Wang SH, Zhao Y (2021) Physical and mechanical properties and related microscopic characteristics of high-temperature granite after water-cooling. Chin J Rock Soil Mech. https://doi.org/10.16285/j.rsm.2020.1383. (**in Chinese**)

Kang FC, Li YC, Tang CA (2021) Grain size heterogeneity controls strengthening to weakening of granite over high-temperature treatment. Int J Rock Mech Min Sci 145:104848. https://doi.org/10.1016/j.ijrmms.2021.104848

Kim K, Kemeny J, Nickerson M (2014) Effect of rapid thermal cooling on mechanical rock properties. Rock Mech Rock Eng 47(6):2005–2019. https://doi.org/10.1007/s00603-013-0523-3

Kumari WGP, Beaumont DM, Ranjith PG, Perera MSA, Avanthi Isaka BL, Khandelwal M (2019) An experimental study on tensile characteristics of granite rocks exposed to different high-temperature treatments. Geomech Geophys Geo-Energy Geo-Resou 5(1):47–64. https://doi.org/10.1007/s40948-018-0098-2

Li SC, Xu XJ, Liu ZY, Yang WM, Liu B, Zang X, Wang ZC, Nie LC, Li JL, Xu L (2014) Electrical resistivity and acoustic emission response characteristics and damage evolution of sandstone during whole process of uniaxial compression. Chin J Rock Mech Eng 33(01):14–23. https://doi.org/10.13722/j.cnki.jrme.2014.01.002. (**in Chinese**)

Li ZH, Wong LNY, Teh CI (2020) Influence of thermal and mechanical loading on development of microcracks in granite. Rock Mech Rock Eng 53(5):2035–2051. https://doi.org/10.1007/s00603-019-02030-0

Li ZWW, Long MC, Feng XT, Zhang YJ (2021) Thermal damage effect on the thermal conductivity inhomogeneity of granite. Int J Rock Mech Min Sci 138:104583. https://doi.org/10.1016/j.ijrmms.2020.104583

Lockner D (1993) The role of acoustic emission in the study of rock fracture. Int J Rock Mech Mining Sci Geomech Abst 30(7):883–899. https://doi.org/10.1016/0148-9062(93)90041-B

Ma X, Wang GL, Hu DW, Liu YG, Zhou H, Liu F (2020) Mechanical properties of granite under real-time high temperature and three-dimensional stress. Int J Rock Mech Min Sci 136:104521. https://doi.org/10.1016/j.ijrmms.2020.104521

Miao ST, Pan PZ, Zhao XG, Shao CY, Yu PY (2021) Experimental study on damage and fracture characteristics of Beishan granite subjected to high-temperature treatment with DIC and AE techniques. Rock Mech Rock Eng 54(2):721–743. https://doi.org/10.1007/s00603-020-02271-4

Niccolini G, Potirakis SM, Lacidogna G et al (2020) Criticality hidden in acoustic emissions and in changing electrical resistance during fracture of rocks and cement-based materials. Materials 13(24):5608. https://doi.org/10.3390/ma13245608

Parkhomenko EI (1982) Electrical resistivity of minerals and rocks at high temperature and pressure. Rev Geophys 20(2):193–218. https://doi.org/10.1029/RG020i002p00193

Parkhomenko EI (2012) Electrical properties of rocks. Springer Science & Business Media.

Rossi E, Kant MA, Madonna C, Saar MO, Rudolf von Rohr P (2018) The effects of high heating rate and high temperature on the rock strength: feasibility study of a thermally assisted drilling method. Rock Mech Rock Eng 51(9):2957–2964. https://doi.org/10.1007/s00603-018-1507-0

Roy KK (2020) Natural electromagnetic fields in pure and applied geophysics. Springer

Shao SS, Ranjith PG, Chen BK (2014) Effect of cooling rate on the mechanical behavior of heated Strathbogie granite with different grain sizes. Int J Rock Mech Min Sci 70:381–387. https://doi.org/10.1016/j.ijrmms.2014.04.003

Sun Q, Zhu S, Xue L (2015) Electrical resistivity variation in uniaxial rock compression. Arab J Geosci 8:1869–1880. https://doi.org/10.1007/s12517-014-1381-3

Tian WL, Yang SQ, Xie LX, Wang ZL (2018) Cracking behavior of three types granite with different grain size containing two non-coplanar fissures under uniaxial compression. Arch Civ Mech Eng 18(4):1580–1596. https://doi.org/10.1016/j.acme.2018.06.001

Tian WL, Yang SQ, Huang YH, Hu B (2020) Mechanical behavior of granite with different grain sizes after high-temperature treatment by grain flow simulation. Rock Mech Rock Eng 53(4):1791–1807. https://doi.org/10.1007/s00603-019-02005-1

Tripathi A, Gupta N, Singh AK, Mohanty SP, Rai N, Pain A (2021) Effects of elevated temperatures on the microstructural, physico-mechanical and elastic properties of Barakar sandstone: a study from one of the world's largest underground coalmine fire region, Jharia. India Rock Mech Rock Eng 54(3):1293–1314. https://doi.org/10.1007/s00603-020-02315-9

Wang F, Konietzky H (2019) Thermo-mechanical properties of granite at elevated temperatures and numerical simulation of thermal cracking. Rock Mech Rock Eng 52(10):3737–3755. https://doi.org/10.1007/s00603-019-01837-1

Wang F, Frühwirt T, Konietzky H, Zhu QY (2019) Thermo-mechanical behaviour of granite during high-speed heating. Eng Geol 260:105258. https://doi.org/10.1016/j.enggeo.2019.105258

Wong LNY, Zhang YH, Wu ZJ (2020) Rock strengthening or weakening upon heating in the mild temperature range? Eng Geol 272:105619. https://doi.org/10.1016/j.enggeo.2020.105619

Xi BP, Wu YC, Wang S, Xiong GM, Zhao YQ (2020) Qinghai province after high temperature thermal damage. Chin J Rock Mech Eng 39(01):69–83. https://doi.org/10.13722/j.cnki.jrme.2019.0182. (**in Chinese**)

Yang SQ, Ranjith PG, Jing HW, Tian WL, Ju Y (2017) An experimental investigation on thermal damage and failure mechanical behavior of granite after exposure to different high temperature treatments. Geothermics 65:180–197. https://doi.org/10.1016/j.geothermics.2016.09.008

Yang SQ, Tian WL, Elsworth D, Wang JG, Fan LF (2020a) An experimental study of effect of high temperature on the permeability evolution and failure response of granite under triaxial compression. Rock Mech Rock Eng 53(10):4403–4427. https://doi.org/10.1007/s00603-019-01982-7

Yang SQ, Hu B, Tian WL (2020b) Effect of high temperature damage on triaxial mechanical failure behavior of sandstone specimens containing a single fissure. Eng Fract Mech 233:107066. https://doi.org/10.1016/j.engfracmech.2020.107066

Yin WT, Feng ZJ, Zhao YS (2021) Effect of grain size on the mechanical behaviour of granite under high temperature and triaxial stresses. Rock Mech Rock Eng 54(2):745–758. https://doi.org/10.1007/s00603-020-02303-z

Zhang F, Zhang YH, Yu YD, Hu DW, Shao JF (2020) Influence of cooling rate on thermal degradation of physical and mechanical properties of granite. Int J Rock Mech Min Sci 129:104285. https://doi.org/10.1016/j.ijrmms.2020.104285

Zhao ZL, Liu ZN, Pu H, Li X (2018) Effect of thermal treatment on Brazilian tensile strength of granites with different grain size distributions. Rock Mech Rock Eng 51(4):1293–1303. https://doi.org/10.1007/s00603-018-1404-6

Zhao XG, Xu HR, Zhao Z, Guo Z, Cai M, Wang J (2019) Thermal conductivity of thermally damaged Beishan granite under uniaxial compression. Int J Rock Mech Min Sci 115:121–136. https://doi.org/10.1016/j.ijrmms.2019.01.014

Zhao F, Shi ZM, Sun Q (2021) Fracture mechanics behavior of jointed granite exposed to high temperatures. Rock Mech Rock Eng 54(5):2183–2196. https://doi.org/10.1007/s00603-021-02393-3

Zhu D, Jing HW, Yin Q, Ding SX, Zhang JH (2020) Mechanical characteristics of granite after heating and water-cooling cycles. Rock Mech Rock Eng 53(4):2015–2025. https://doi.org/10.1007/s00603-019-01991-6

Zhu ZN, Ranjith PG, Tian H, Jiang GS, Dou B, Mei G (2021) Relationships between P-wave velocity and mechanical properties of granite after exposure to different cyclic heating and water cooling treatments. Renew Energy 168:375–392. https://doi.org/10.1016/j.renene.2020.12.048